American Mineralogist, Volume 97, pages 1708–1713, 2012

Solubility of xenotime in a 2 *M* HCl aqueous fluid from 1.2 to 2.6 GPa and 300 to 500 °C

Elizabeth A. Tanis,[1,2,*,†] Adam Simon,[1,2,†] Oliver Tschauner,[1,2] Paul Chow,[3] Yuming Xiao,[3] Gouyin Shen,[3] John M. Hanchar,[4] and Mark Frank[5]

[1]High Pressure Science and Engineering Center, University of Nevada, Las Vegas, Nevada 89154-4010, U.S.A.
[2]Department of Geoscience, University of Nevada, Las Vegas, Nevada 89154-4010, U.S.A.
[3]HPCAT, Geophysical Laboratory, Carnegie Institute of Washington, Argonne, Illinois 60439, U.S.A.
[4]Department of Earth Sciences, Memorial University of Newfoundland, St. John's, Newfoundland A1B 3X5, Canada
[5]Department of Geology and Environmental Geosciences, Northern Illinois University, DeKalb, Illinois 60115, U.S.A.

Abstract

Constraining mass transfer of the rare earth elements (REE) and high field strength elements (HFSE) from subducted oceanic crust and metasediments to the mantle wedge is fundamental toward interpreting processes that affect trace element mobility in subduction zone environments. Experimental studies of the partitioning of trace elements involving aqueous fluids at *P-T* conditions appropriate for slab-mantle wedge conditions are complicated by the difficulties in retrieving the fluid. Here we present the results from an application of an in situ technique that permits quantitative determination of element concentrations in aqueous fluid at geologically relevant supercritical conditions. We focus on pressures and temperatures appropriate for devolatilization-induced element transfer in subduction zone environments, and conditions obtained during regional metamorphism. In this study, we used a hydrothermal diamond-anvil cell (HDAC) and in situ synchrotron X-ray fluorescence (SXRF) to quantify the concentration of Y, an important trace element often used as a proxy for the heavy REE in geologic systems, in a xenotime-saturated 2 *M* HCl-aqueous fluid at 1.19 to 2.6 GPa and 300–500 °C. At these pressures and temperatures the solubility of yttrium ranges from 2400 to 2850 ppm. We find that the concentration of Y decreases with increasing fluid density. These new data, combined with published data generated from experiments done at lower pressure, in fluids of nearly identical composition and also NaCl-H_2O fluids, constrain the effects of pressure and temperature on the ability of aqueous fluid containing Cl to scavenge and transport Y and, by analogy, the HREE. Although the physical properties of Y are similar to the high field strength elements, Y exhibits geochemical behavior that is analogous to the heavy rare earth elements (HREE).

Keywords: Synchrotron, subduction, aqueous fluid, metasomatism, fluid transfer, hydrothermal diamond-anvil cell, xenotime, rare earth elements, yttrium

Introduction

Arc volcanoes and their plutonic counterparts are the surface and crustal manifestations, respectively, of processes originating with the transfer of aqueous fluids (±melt) from subducted ocean lithosphere and overlying metasediments to the mantle wedge. These fluids induce partial melting of the mantle wedge (e.g., Aizawa et al. 1999) and have been postulated to contribute to the fractionation of trace elements, which in turn may leave an imprint on the trace element composition of the arc volcanic rocks (Kay 1984; Bebout et al. 1999). It has also been proposed that the fluid triggers partial melting of the mantle and that trace element patterns are controlled by the partitioning of elements between the ascending melt and mantle (Kessel et al. 2005). Quantifying the nature of fluid (±melt) transfer at the pressure and temperature conditions appropriate for the subduction zone environment is crucial for evaluating the role of fluids in such opposing models. More generally, quantitative data that constrain the trace element-scavenging ability of aqueous fluid at elevated pressure and temperature will lead to a better understanding of the recycling of elements between ocean lithosphere, metasediments, mantle wedge, and crust. To this end, significant effort has been made to constrain the relative mobility of major, minor, and trace elements in fluid-bearing magmatic and metamorphic systems to understand the origin of variation in absolute element abundances and element ratios.

Most previous studies designed to quantify the partitioning of elements between aqueous fluid and minerals or melt at elevated pressure and temperature have been of the recovery type. Element distribution and concentrations in such experiments were determined by measuring the change in the concentration of a particular element in the starting and final phase assemblages. In the past decade, efforts have been made to develop an in situ technique that permits quantification of element distribu-

* E-mail: eatanis@umich.edu
† Present address: Department of Earth and Environmental Sciences, University of Michigan, Ann Arbor, MI 48109-1005, U.S.A.

0003-004X/12/0010–1708$05.00/DOI: http://dx.doi.org/10.2138/am.2012.4009

tion between fluid and minerals. These efforts have focused on the use of an externally heated diamond-anvil cell (DAC) as the pressure vessel. Sanchez-Valle et al. (2003) measured the solubility of strontianite in H_2O by using a DAC to subject the charge to 0.4 to 3.6 GPa and from 25 to 250 °C, respectively. They directly measured the concentration of Sr by using in situ synchrotron X-ray fluorescence (SXRF). Those authors reported that the dissolution of strontianite into the fluid increased as a function of increasing pressure and temperature. Schmidt et al. (2006) investigated the solubility of zircon in $H_2O + HCl \pm SiO_2$ fluids at temperatures between 200 and 500 °C and pressures of ~2 GPa by using a hydrothermal diamond-anvil cell (HDAC) and in situ time-resolved synchrotron-radiation XRF analyses. They reported that the solubility of Zr decreases with increasing temperature. Schmidt et al. (2007) used the HDAC and in situ SXRF to quantify the solubility of monazite in aqueous fluid at 250 to 800 °C and a maximum pressure of 2 GPa, and the solubility of xenotime in aqueous fluid at 250 to 600 °C and a maximum pressure of 1.32 GPa. Their HDAC configuration was designed with a cylindrical recess in the lower anvil that permitted collection of the element specific fluorescence signal specifically from fluid in the recessed part of the chamber. Manning et al. (2008) measured rutile solubility in $NaAlSi_3O_8$-bearing aqueous fluids at 0.31 to 1.23 GPa and 600 to 800 °C. They also used an HDAC configuration that contained one anvil that was modified with a recess. Manning et al. (2008) reported that the solubility of rutile was strongly positively correlated with the concentration of dissolved $NaAlSi_3O_8$. Stechern et al. (2009) measured the solubility of zircon in aqueous fluid that contained variable concentrations of dissolved HCl and $Na_2Si_2O_5$ from 0.33 to 0.63 GPa and 500 to 750 °C; they also used a recessed-anvil HDAC. Their results showed no correlation between the solubility of zircon and the concentrations of HCl and $Na_2Si_2O_5$ in the fluid.

There have been two high-pressure studies on the solubility of yttrium in aqueous fluid. Schmidt et al. (2007) used the SXRF technique with an HDAC. Their study reported data that constrain the solubility of xenotime in a 1.88 *M* HCl aqueous fluid at pressures from 0.0045 to 1.32 GPa and temperatures from 250 to 600 °C, respectively. The results indicate that the solubility of yttrium in the fluid increases from 220 to 4231 ppm with increasing pressure and temperature. Tropper et al. (2011) also studied the solubility of xenotime in NaCl-bearing aqueous fluid, at variable NaCl concentrations, at 1 GPa and 800 °C by using the recovery technique and a piston-cylinder apparatus to generate pressure. Their results indicate that the concentration of yttrium in NaCl-bearing aqueous fluid increases with increasing NaCl concentration at constant pressure and temperature. Pressure, temperature, and fluid composition all contribute to the structure and density of the fluid and thus, affect the activity and partitioning of yttrium. In this study, we constrained the behavior of Y in aqueous fluid as a function of these parameters to evaluate the hypothesized role that aqueous fluid plays in moderating the mobility of Y and, by analogy, the heavy rare earth elements (HREE) in subduction zone environments.

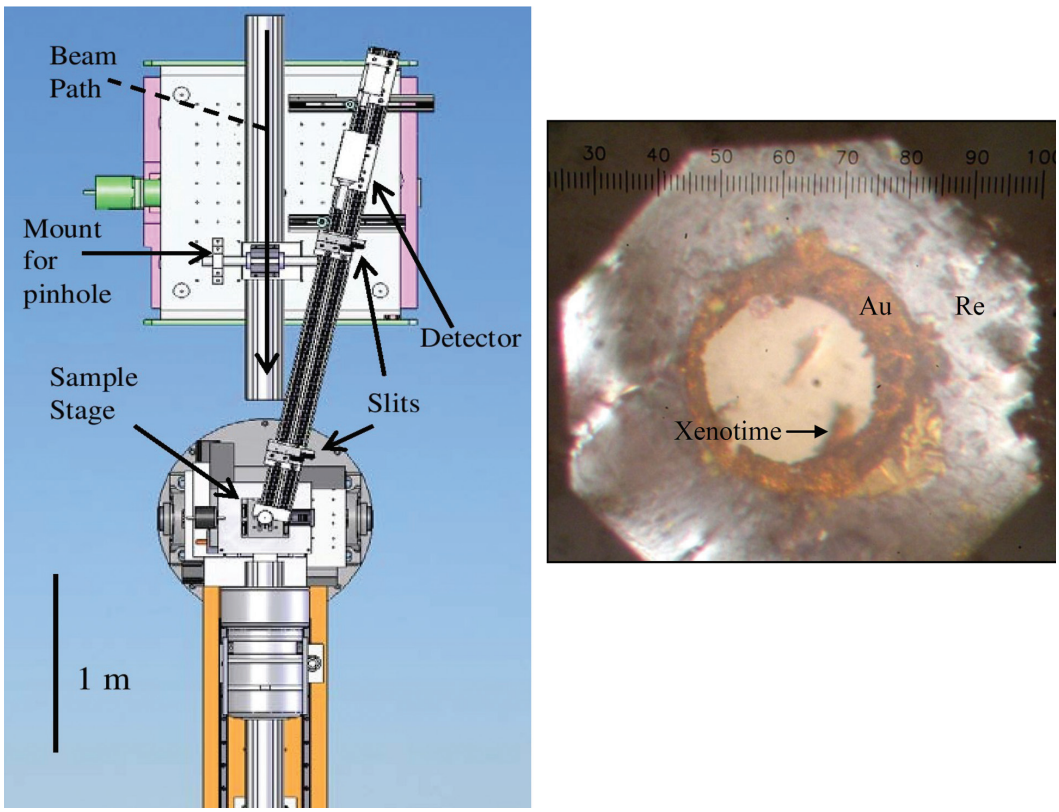

FIGURE 1. (**left**) The experimental setup at 16 ID-D features a 170° back scatter orientation. The location of the detector, slits, sample stage and the X-ray beam path are noted in the figure. A CCD X-ray detector is mounted behind the sample stage. (**right**) The Au-lined Re gasket. (Color online.)

EXPERIMENTAL METHODS

The synthetic end-member xenotime (YPO_4) crystals used in this study were prepared in the experimental geochemistry laboratory at Memorial University of Newfoundland following the method described in Hanchar et al. (2001). Briefly, high-purity Y_2O_3 and ammonium dihydrogen phosphate ($NH_4H_2PO_4$), obtained from Alfa Aesar, were thoroughly mixed in stoichiometric proportions of 1.5 mol% Y_2O_3; and 3 mol% $NH_4H_2PO_4$, in an HNO_3-cleaned agate mortar and pestle under absolute ethanol and allowed to dry. Once dried, the powders were mixed under absolute ethanol with the fluxing agents Li_2MoO_4 and MoO_3 in the following proportions: 86 mol% MoO_3; 9.5 mol% Li_2MoO_4; and the 4.5 mol% mixture of Y_2O_3 and $NH_4H_2PO_4$ mixture mentioned above and allowed to dry. The mixture was then transferred to a clean platinum crucible with a tightly fitted Pt lid. The crucible was lowered into the "hot spot" of a preheated (1250 °C) Deltech $MoSi_2$ vertical tube furnace for seven days, at constant temperature, permitting the flux to evaporate. When xenotime saturation was reached, the xenotime crystals began to grow in the residual flux. Using a type S control thermocouple, the temperature in the hot spot was measured to within ±5 °C. Upon completion of the synthesis, no residual flux remained in the crucible. The xenotime crystals were simply removed from the Pt crucible with tweezers, and cleaned in concentrated HNO_3.

The SXRF experiments were done at undulator beamlime 16-IDD (HPCAT) at the Advanced Photon Source (APS) synchrotron facility at Argonne National Laboratory. The incident beam energy was 20.1 keV. The beam was focused to 35 by 50 µm full-width at half maximum (FWHM) by using a pair of Kirkpatrick-Baez mirrors and a 100 µm round pinhole was used just before the HDAC to clean up the tails of the incident beam, which contained a flux of 1.14×10^{12} photons/s/mm^2. The incident beam was projected through the diamonds of the HDAC into the sample chamber. The fluorescence from the sample was collected in a 170° backscattering geometry by using a Vortex-EX silicon drift detector that was positioned ~0.8 meters from the sample (Fig. 1, left). To reduce the background, a pair of large collimating slits was placed before the detector, therefore requiring more distance from the sample. The energy channels of the multi-channel analyzer were calibrated with Fe-55, Co-57, and Cd-109 radioactive sources. The position and aperture of the detector was optimized by using a powder Y_2O_3 commercial plasma-grade standard that was centered on the experimental stage.

The HDAC that was used in the current study described in detail by Bassett et al. (1993) was equipped with two opposing 500 µm culet diamonds, and had resistive molybdenum wires coiled around a tungsten carbide seat that supported each diamond anvil. Two K-type (NiCr-NiAl) thermocouples were used to measure temperature, one on each diamond. The HDAC was heated resistively by using variable transformers that facilitated flexible heating rates and allowed us to maintain temperature to ±5 °C. The HDAC had been previously calibrated up to 645 °C by observing the melting point of CsCl, which was found to be within 5 °C of the thermocouple reading. The HDAC has been calibrated up to 800 °C by observing the melting point or phase transition of $NaNO_3$, CsCl, and NaCl, and measured temperatures were systematically lower by ~0.85% over the entire range studied (Kerrigan 2011). A 1% H_2-Ar gas mixture was flowed constantly through the HDAC during the measurements to prevent corrosion of the diamonds and the heaters.

A laser-drilled Re gasket was filled with Au, compressed, and re-drilled; hence forming a Au liner that acted as an inert barrier to minimize, if not altogether eliminate, chemical interaction between the experimental aqueous fluid and the Re gasket (Fig. 1, right). The Au served also as an in situ reference material for pressure calibration. X-ray diffraction (XRD) patterns of gold were recorded by using a MAR 165 CCD detector in the forward scattering direction during the experiments. The patterns were integrated and corrected for geometric distortions using Fit2D (Hammersley 1997). A NIST standard CeO_2 pattern was collected and used to calibration. A synthetic, end-member, single xenotime crystal that measured $15 \times 15 \times 10$ µm was loaded into the HDAC, and then 2 *M* HCl-aqueous fluid was added to the sample chamber by using a micro syringe (Fig. 1, right). The HDAC was centered on the sample stage and then rotated into a position that prevented any fluorescence from the xenotime crystal from entering the detector.

The HDAC was heated at experimental *P* to 300 °C, and pressure was monitored by collecting XRD patterns of Au throughout the run using the pressure scale by Dorogokupets and Dewaele (2007). Fluorescence spectra were collected iteratively in 300 s intervals. We assessed equilibrium by evaluating the time-dependence of the fluorescence signal. Once the Y peak area, at a unique pressure and temperature condition, became time-invariant, it was interpreted to reflect the

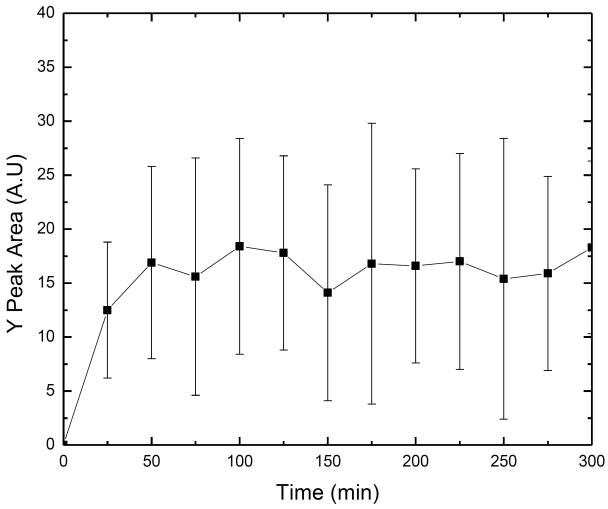

FIGURE 2. The integrated peak area from the sum of 30 min intervals at 300 °C plotted as a function of time. Once the Y peak area, at a unique pressure and temperature condition, became time-invariant it was interpreted to reflect the attainment of steady-state conditions and proximity to chemical equilibrium. The error bars are determined by propagating the uncertainties in the fitting procedure to the integrated peak area.

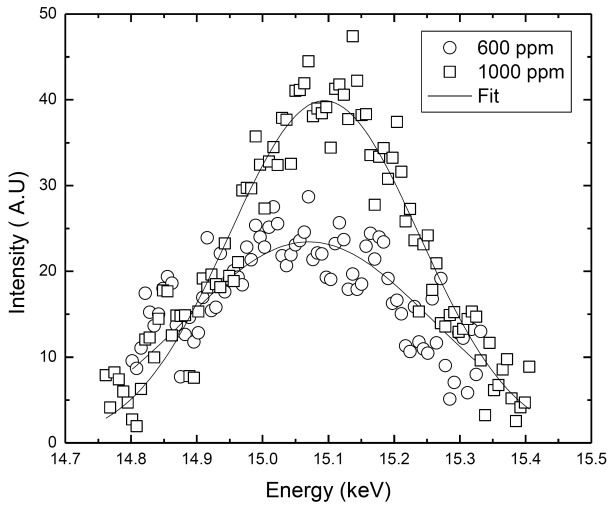

FIGURE 3. The summed XRF spectra of the Y standard solutions. The squares represent 1000 ppm Y and the circles represent 600 ppm yttrium. The solid lines represent the fit of the curves.

TABLE 1. Experimental conditions

Run	1	2	3	4	5
Temperature (°C)	310 (±2.6)	450 (±3.8)	500 (±4.3)	430 (±3.6)	300 (±2.5)
Pressure (GPa)	2.6 (±0.1)	2.17 (±0.1)	2.33 (±0.2)	1.86 (±0.15)	1.19 (±0.15)
Cumulative run duration (min)	0–300	300–600	600–900	900–1060	1060–1420
Concentration of Y in fluid (weight ppm)	2400 (±215)	2450 (±222)	2575 (±231)	2850 (±258)	2700 (±244)
HCl (*M*)	2.0	2.0	2.0	2.0	2.0

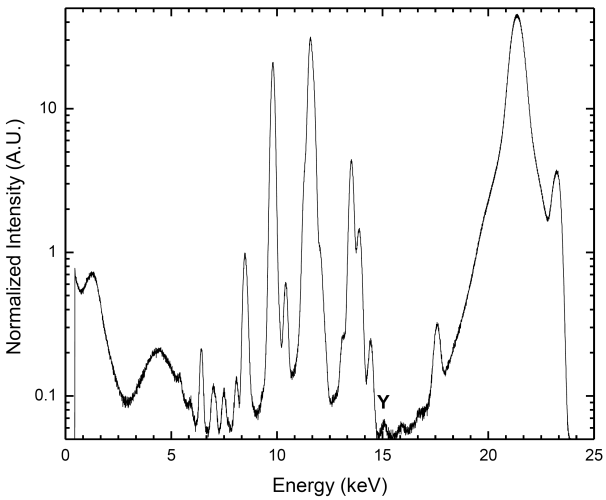

FIGURE 4. The summed and normalized XRF spectra of the 1000 ppm Y standard solution. The Y peak was sufficiently distinct from the Compton scattering signal arising from diamond, which justified a local linear background fit.

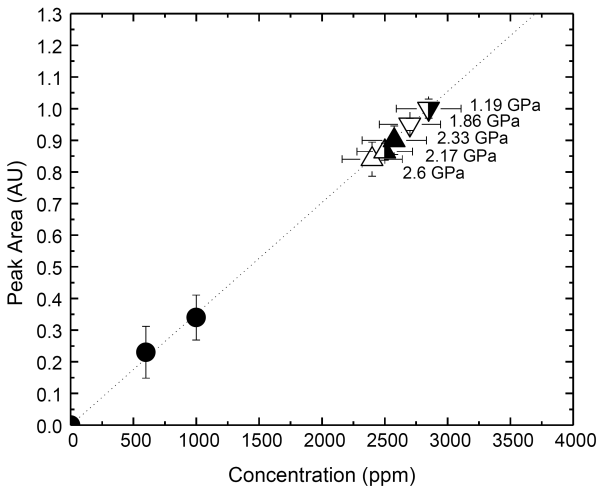

FIGURE 5. The integrated peak area of the Y standard solutions (black dots) demonstrate a linear relationship (dotted line) between concentration and peak area. The upward pointing triangles represent data that were collected as temperature was increased from ambient to run conditions. The downward pointing triangles represent data that were collected after temperature was decreased. See text for details. The open symbols represent 300 °C, half-filled triangles represent 450/430 °C, and the solid triangle represents 500 °C.

attainment of steady-state conditions and proximity to chemical equilibrium. This is shown in Figure 2. This took approximately 30–40 min at each unique *P-T* point. The time to reach steady state is consistent with observations reported by Manning et al. (2008), Schmidt et al. (2007), and Sanchez-Valle et al. (2003). After steady-state conditions were achieved, spectra were collected in 300 s intervals for ~3 h. The temperature was then increased to 450 °C, and subsequently to 500 °C, and the data collection procedure was repeated at each temperature. The temperature was then decreased from 500 to 450 °C and subsequently to 300 °C following the same data collection protocol. The experimental results are reported in Table 1. During heating and cooling, there is some relaxation of the HDAC. This can cause deformation in the gasket sample chamber and result in a slight change in pressure. We observed this change and, therefore, measured pressure before and after each sequence of fluorescence data were collected.

After collecting the experimental spectra, the xenotime and fluid were removed and the gasket was cleaned. The detector response was found to be linear up to1000 ppm by using two different calibrant solutions (600, 1000 ppm) of Y in the HDAC. Previous SXRF studies reported that a valid fluorescence calibration was achieved by a multi-point calibration (Sanchez-Valle et al. 2003) as well as a single-point calibration (Manning et al. 2008). Sanchez-Valle et al. (2004) confirmed the validity of the calibration technique as a function of pressure and temperature by analyzing Rb and Sr up to 3.2 GPa and 200 °C. They found that there was no characteristic change in the $K\alpha$ fluorescence peaks. In these experiments a 600 and 1000 ppm Y standard aqueous solutions (prepared from an Alfa Aesar plasma standard) were loaded into the same gasket held in the same HDAC. This was done to ensure that the fluorescence spectra collected from the standards and the experimental fluid originated from the same excitation volume. The spectra for the standard solutions were collected in 300 s intervals for a total time of 3600 s (Fig. 3). Note that prior to the experiments, fluorescence spectra of the empty HDAC were collected and Y was not detected. This established a zero concentration for the standard calibration. Self-absorption of Y was assessed by evaluating the photoionization cross-section energy at the Y absorption edges and found that self absorption is negligible.

The fluorescence spectra from the standard solutions and high *P-T* experiments were each separately summed, and normalized to transmitted beam flux and time. We monitored beam flux and used this to normalize fluorescence spectra to account for beam flux variations. The background and area of the Y fluorescence peak was fit by using Fityk (Wojdyr 2010). The Y peak was sufficiently distinct from the Compton scattering signal arising from diamond, which justified a local linear background fit (Fig. 4). The background was determined by selecting the minimum point from each side of the Y peak and then subtracting the linear fit between the two points. The background subtracted integrated peak area for the 600 and 1000 ppm Y standards and the zero parts per million Y reference point were used to define a linear calibration curve that was used to calculate Y concentrations in the experimental fluid (Fig. 5). The weighted uncertainties for the experimental concentrations were calculated from peak fitting of the experimental data, and by propagating the uncertainty from the standards, which were composed from the uncertainty of the standards peak fit and the calibration curve.

RESULTS AND DISCUSSION

Xenotime solubility in supercritical aqueous fluid is relatively insensitive to changes in pressure and temperature at the experimental conditions in the current study (Fig. 6 and Table 1). However, when plotted with the xenotime solubility data from Schmidt et al. (2007) (Figs. 6a and 6b), conclusions can be drawn about the effect of pressure and temperature. Their data were collected at the same temperatures as those of the current study, but at lower pressures, between 0.01 and 0.29 GPa. The fluid composition in the current study (2 *M* HCl) was nearly identical to that reported by Schmidt et al. (2007; 1.8 *M* HCl). The combined data indicate that the effect of pressure on the solubility of xenotime in aqueous fluid decreases with increasing temperature. At 300 °C, the concentration of yttrium in aqueous fluid increases from 500 to ~2500 ppm as pressure increases from 0.01 to ~2 GPa, respectively. At 450 °C, the concentration of yttrium in aqueous fluid increases from 1760 to ~2500 ppm as pressure increases from 0.2 to ~2 GPa, respectively. At 500 °C, the concentration of yttrium in aqueous fluid is 2355 ppm at 0.29 GPa and 2575 ppm at 2.3GPa.

There is an ongoing discussion about the liquid/liquid structure transition in water around 1 GPa because the density of water changes non-linearly (Kawamoto et al. 2004; Strassle et al. 2006). Changes in the first coordination shell of water may occur in the fluid state and affect the solubility of xenotime and the way Y is coordinated by Cl^- and water molecules at pressures above 1 GPa. Therefore, it is interesting to look at the evolution of xenotime solubility as a function of density of

water. In this study, the density of water was calculated from the equation of state of Abramson and Brown (2004). The log density of water versus log molality YPO_4 plot (Fig. 6c) reveals that, as density increases, the solubility of xenotime in the fluid decreases. This observation for the solubility of xenotime is opposite that of trends reported and discussed in Dolejs and Manning (2010) for minerals such as apatite, rutile, quartz,

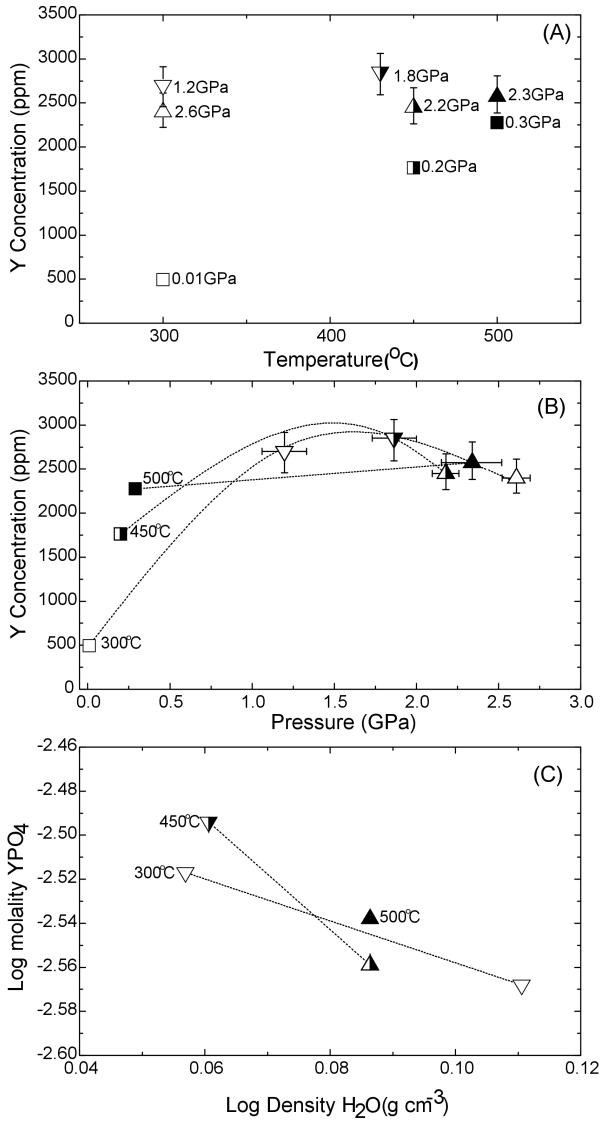

FIGURE 6. The SXRF experimental data for xenotime solubility in 2 *M* HCl aqueous fluid quantified as a function of temperature (**a**), pressure (**b**), and calculated fluid density (**c**). These data from the current study (triangles) are combined with the xenotime solubility data of Schmidt et al. (2007) (squares) in figures **a** and **b**. The upward pointing triangles represent data collected as temperature was increased from ambient to run conditions. The downward triangles represent data that were collected as temperature was decreased. The open symbols represent 300 °C, half filled are 450/430 °C, and solid are 500 °C. The dashed lines are to guide the eye between the isotherms. The combined data indicate that the effect of pressure on the solubility of xenotime in aqueous fluid decreases with increasing temperature.

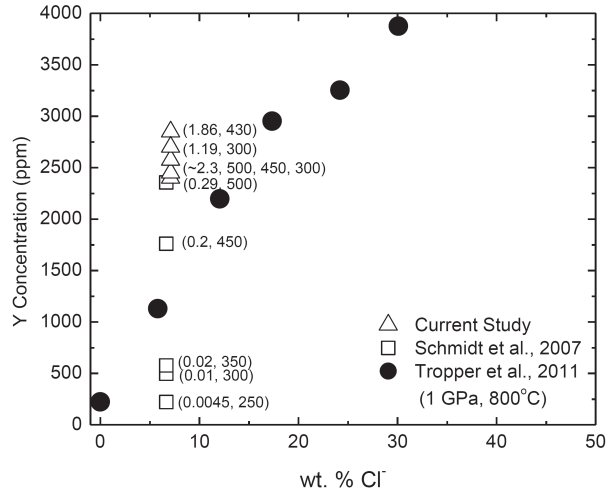

FIGURE 7. The experimental data for xenotime solubility in aqueous fluid plotted as a function of the Cl concentration of the fluid. The Schmidt et al. (2007) study (squares) covers a *P-T* range of 0.04 to 1.3 GPa and 250 to 600 °C and the Cl was added in the form of HCl. In the Tropper et al. (2011) study (filled circles) the Cl was added in the form of NaCl and all experiments were at 1 GPa and 800 °C. The current study (triangles) covered a *P-T* range of 1.19 to 2.6 GPa and 300 to 500 °C. Pressure and temperature are provided (GPa, °C) for data for the current study and Schmidt et al. (2007).

corundum, calcite, fluorite, and portlandite, which display an increase in their solubility in aqueous fluid with increasing temperature and fluid density. We hypothesize that the changes in density and the structure of water at the pressure and temperature conditions of the current study may affect the affinity of Y and Cl^- to coordinate with one another in the fluid. This will be investigated in a future study.

The xenotime solubility data from the current study are plotted in Figure 7 as a function of the total chloride concentration in the fluid. Also plotted are data from Schmidt et al. (2007) and data from Tropper et al. (2011). Whereas in the present study and the study of Schmidt et al. (2007), Cl was added as HCl, Tropper et al. (2011) added Cl as NaCl. In comparison, these data place first order constraints on the role of HCl vs. NaCl to dissolve xenotime. The data indicate that HCl, relative to NaCl, has a greater influence on the solubility of xenotime. For example, at 1.19 GPa and 300 °C, an aqueous fluid that contains ~8 wt% Cl in the form of HCl can dissolve 2700 ppm yttrium. Whereas, Tropper et al. (2011) reported that at 1 GPa and 800 °C, an aqueous fluid requires ~16 wt% Cl in the form of NaCl to dissolve ~2700 ppm yttrium. This observation suggests that fluid composition, in addition to the role of fluid density, as discussed above, plays a critical role in dissolving xenotime. If the following two reactions describe dissolution of xenotime in HCl and NaCl bearing fluid, then the available data indicate that the equilibrium constant for reaction 1 is much greater than for reaction 2 in accordance with expectations from aqueous chemistry at ambient conditions.

$$YPO_{4(s)} + 3HCl_{(aq)} \rightarrow YCl_{3(aq)} + H_3PO_{4(aq)} \quad (1)$$
$$YPO_{4(s)} + 3NaCl_{(aq)} \rightarrow YCl_{3(aq)} + Na_3PO_{4(aq/s)}. \quad (2)$$

In the absence of an extensive data set for the partitioning of trace elements at the pressure and temperature where aqueous fluids evolve from the subducted slab into the mantle wedge, the data presented in this study can be used to illustrate the potential role of aqueous fluid at moderating trace element ratios in natural systems. If we take the results published by Sanchez-Valle et al. (2003) for the solubility of strontianite ($SrCO_3$) in aqueous fluid from 0.4 to 3.6 GPa and 25 to 250 °C as representative for the combined pressure and temperature effects on the solubility of the light ion lithophile elements (LILE) in aqueous fluids, and consider Y as a representative of the HREE, the combined data suggest that the pressure effect on the ability for aqueous fluid to scavenge the LILE is much greater than HREE. For instance, Sanchez-Valle et al. (2003) reported a solubility of Sr of ~15 500 ppm (1.55 wt%) in pure H_2O at 3.6 GPa and 252 °C. The solubility of yttrium at similar conditions (2.6 GPa, 310 °C) measured in the current study in 2 *M* HCl aqueous fluid is ~2400 ppm (0.24 wt%). While strontianite is not the LILE bearing phase in subduction zone settings, the experimental data yield a model Sr/Y mass ratio of ~6.

As discussed above, fluid chemistry plays a major role in controlling the solubility of xenotime, and likely strontianite, in aqueous fluid. Therefore, considering the strong effect of HCl on the solubility of xenotime, the solubility of Sr is expected to increase in acidic solutions. Thus the model Sr/Y ratio most likely underestimates Sr/Y ratios in natural fluids. Nonetheless, the combined data suggest that the release of aqueous fluid from slab material may efficiently fractionate LILE from HREE, which is consistent with observations of the LILE/HREE ratios in arc magmas where aqueous fluid has been postulated to play a role in stimulating melting of the sub-arc mantle.

Acknowledgments

This study was partially sponsored by the National Nuclear Security Administration (NNSA) under the Stewardship Science Academic Alliances program through DOE Cooperative Agreement no. DE-FC52-06NA27684. HPCAT Sector 16 of the Advanced Photon Source at Argonne National Laboratory is supported by DOE-BES, DOE-NNSA, DOD-TACOM, and the W.M. Keck Foundation. We acknowledge COMPRESS and GSECARS for the use of the laser drilling system. The Advanced Photon Source is supported by the U.S. Department of Energy, Office of Science, Office of Basic Science, under Contract No. DE-AC02-06CH11357. We thank Eric Rod for providing the beamline schematic image. J.M.H. thanks the Canadian Natural Sciences and Research Council (NSERC) for partial support for this research in the form of a Discovery Grant, and Memorial University of Newfoundland, for additional financial support for this project. We thank Craig Manning and an anonymous reviewer for detailed constructive comments that helped significantly to improve the manuscript.

References cited

Abramson, E.H. and Brown, J.M. (2004) Equation of state of water based on speeds of sound measured in the diamond-anvil cell. Geochimica et Cosmochimica Acta, 68, 1827–1835.

Aizawa, Y., Tatsumi, Y., and Yamada, H. (1999) Element transport during dehydration of subducting sediments: implications for arc and ocean island magmatism. The Island Arc, 8, 38–46.

Bassett, W.A., Shen, A.H., Bucknum, M., and Chou, I.-M. (1993) A new diamond anvil cell for hydrothermal studies to 2.5 GPa and from −190 to 1200 °C. Reviews of Scientific Instruments, 64, 2340–2345.

Bebout, G.E., Ryan, J.G., Leeman, W.P., and Bebout, A.E. (1999) Fractionation of trace elements by subduction zone metamorphism—effect of convergent-margin thermal evolution. Earth and Planetary Science Letters, 171, 63–81.

Dolejs, D. and Manning, C.E. (2010) Thermodynamic model for mineral solubility in aqueous fluids: theory, calibration and application to model fluid-flow systems. Geofluids, 10, 20–40.

Dorogokupets, P.I. and Dewaele, A. (2007) Equations of state of MgO, Au, Pt, NaCl-B1, and NaCl-B2: Internally consistent high-temperature pressure scales. High Pressure Research: An International Journal, 27, 431–446.

Hammersley, A.P. (1997) ESRF Internal Report, ESRF97HA02T, "FIT2D: An Introduction and Overview."

Hanchar, J.M., Finch, R.J., Hoskin, P.W.O., Watson, E.B., Cherniak, D.J., and Mariano, A.N. (2001) Rare earth elements in synthetic zircon: Part 1. Synthesis, and rare earth element and phosphorus doping. American Mineralogist, 86, 667–680.

Kawamoto, T., Ochiai, S., and Kagi, H. (2004) Changes in the structure of water deduced from the pressure dependence of the Raman OH frequency. Journal of Chemical Physics, 120, 5867–5870.

Kay, R.W. (1984) Elemental abundances relevant to identification of magma sources. Philosophical Transactions of the Royal Society of London, Series A., 310, 535–547.

Kessel, R., Schmidt, M.W., Ulmer, P., and T. Pettke. (2005) Trace element signature of subduction zone fluids, melts, and supercritical liquids at 120-180 km depth. Nature, 437, 724–727.

Kerrigan, R.J. (2011) Reaction Rates and textural development of hydrolysis reactions in the system MgO-SiO_2-H_2O. Dissertation, University of Maryland.

Manning, C.E., Wilke, M., Schmidt, C., and Cauzid, J. (2008) Rutile solubility in albite-H_2O and $Na_2Si_3O_7$-H_2O at high temperatures and pressures by in-situ synchrotron radiation micro-XRF. Earth and Planetary Science Letters, 272, 730–737.

Sanchez-Valle, C., Martinez, I., Daniel, I., Philippot, P., Bohic, S., and Simionovici, A. (2003) Dissolution of strontianite at high *P-T* conditions: An in situ synchrotron X-ray fluorescence study. American Mineralogist, 88, 978–985.

Sanchez-Valle, C., Daniel, I., Martinez, I., Simionovici, A., and Reynard, B. (2004) Progress in quantitative elemental analyses in high *P-T* fluids using synchrotron X-ray fluorescence (SXRF). Journal of Physics: Condensed Matter, 16, 1197–1206.

Schmidt, C., Rickers, K., Wirth, R., Nasdala, L., and Hanchar, J. (2006) Low-temperature Zr mobility: An in situ synchrotron-radiation XRF study of the effect of radiation damage in zircon on the element release in H_2O + HCl ± SiO_2 fluids. American Mineralogist, 91, 1211–1215.

Schmidt, C., Rickers, K., Bilderback, D.H., and Huang, R. (2007) In situ synchrotron-radiation XRF study of REE phosphate dissolution in aqueous fluids to 800 °C. Lithos, 95, 87–102.

Stechern, A., Wilke, M., Schmidt, C., Rickers, K., Pascarelli, S., Manning, C.E. (2009) XAFS measurements on Zr in aqueous fluids at high pressures and temperatures using a modified hydrothermal diamond-anvil cell. Journal of Physics: Conference Series, 190, art. no. 012058.

Strassle, T., Saitta, A.M., Le Godec, Y., Hamel, G., Klotz, S., Loveday, J.S., and Nelmes, R.J. (2006) Structure of dense liquid water by neutron scattering to 6.5 GPa and 670 K. Physcal Review Letters, 96, 067801.

Tropper, P., Manning, C.E., and Harlov, D.E. (2011) Solubility of $CePO_4$ monazite and YPO_4 xenotime in H_2O and H_2O–NaCl at 800 °C and 1 GPa: Implications for REE and Y transport during high-grade metamorphism. Chemical Geology, 282, 58–66.

Wojdyr, M. (2010) *Fityk*: a general-purpose peak fitting program, Journal of Applied Crystallography, 43, 1126–1128.

Manuscript received September 23, 2011
Manuscript accepted June 6, 2012
Manuscript handled by Wendy Mao